

First-principles theoretical study on the electronic properties of the $B32$ intermetallic compound LiAl^\dagger

Alex Zunger*

Department of Physics and Astronomy and Material Research Center, Northwestern University, Evanston, Illinois 60201

(Received 27 June 1977)

The electronic properties of the ordered LiAl crystal are studied within the self-consistent (non-muffin-tin) numerical-basis-set approach to the local-density formalism. The material appears to be electronically a semimetal with an electron pocket near X (along Δ) and a hole pocket at Γ . The band structure and density of states have characteristics similar to that of the tetrahedrally bonded IV-IV semiconductors (LiAl has a T_d site symmetry); however, the indirect $\Gamma_{25'}-X_1$ band gap (which decreases progressively as one goes along the diamond, Si, Ge, and α -Sn series) becomes *negative* in LiAl . A study of charge redistribution effects indicates that while the Li-Al bond is an ionically polarized covalent bond, the Al-Al bonds are metalliclike and the Li-Li bonds are essentially nonbonding. Wave-function population analysis indicates that the bottom of the occupied valence band is of predominantly Li $2s$ character (hybridized with Al $3s$), while at higher energies the Li $2s$ character is reduced in favor of the Li and Al p character, which are dominant around the Fermi energy. The main intrasite-charge-redistribution effects involve pronounced Li $2s$ to Li $2p$ promotion (with a smaller s - p promotion on the Al site) while the intersite (ionic) redistribution effects are found to be small. The observed trends in the measured Knight shifts (relative to the pure constituent metals) as well as the small paramagnetism and its dependence on the Li concentration are discussed in terms of these bonding effects. The abrupt changes in the differential electrical resistivity at $\sim 100^\circ\text{K}$ is tentatively assigned to a structural instability induced by electron-hole interaction effects.

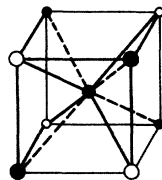
I. INTRODUCTION

We report in this paper a theoretical study on the electronic structure of solid LiAl , the prototype of the $B32$ structure (Zintl-phase)¹ intermetallic compounds. Recent interest in developing batteries capable of high-energy density,² has led to the use of LiAl as anodic material due to its stability and relative high electrochemical activity. The material crystallizes³ in a body-centered-cubic lattice made up of two interpenetrating diamond sublattices of Li and Al (Fig. 1). Each atom has a tetrahedral T_d site symmetry and four nearest neighbors of each type, leading to a situation where all Li-Li and Al-Al bond distances (which are equal to the Li-Al distance) are some 10% and 4% shorter than in the pure Li and Al metals, respectively.

Nuclear-magnetic-resonance (NMR) measurements of the ^7Li dipolar temperature line width narrowing as well as Al^{27} quadrupolar effects³⁻⁵ have indicated over a wide temperature range the presence of a substantial amount of Li vacancies even in stoichiometric samples. The temperature dependence of the dipole and quadrupole contributions to the linewidths and spin-lattice relaxation rates suggests a very low activation energy of 0.13–0.15 eV for the sources of the fluctuating dipolar fields and the electric field gradients in the system [compared with 0.52 eV in pure Li (Ref. 6) and 1.45 eV for the Li in Al (Ref. 7)]. This suggests that the vacancies do not have to form thermally but that only their migration energy

is thermally induced. Such permanent vacancy concentration seems to occur in other defect lattices such as NiAl .^{8,9} Resistivity measurements¹⁰ on LiAl indicate weak metallic conductivity with an abrupt increase in resistivity and change in the slope with temperature for Li-deficient (i.e., higher vacancy content) samples. Similarly, susceptibility measurements^{11,12} have indicated a very low paramagnetic contribution with a sharp decrease towards diamagnetism for Li-rich samples. Knight-shift measurements³ have shown a drastic decrease in both Li and Al shifts relative to the pure metals while NMR studies on the T_1 spin-lattice relaxation time^{4,5} have indicated a vanishing conduction-electron contribution, in contrast to the situation in the pure metals.

We have performed a fully self-consistent band study on the ideal LiAl structure within the local-density formalism (LDF),^{13,14} using our previously developed numerical basis set (non-muffin-tin) self-consistent band method.^{15,16} An extended numerical basis set was used and no shape approxi-



○ Li
● Al

FIG. 1. Crystal structure of the $B32$ Zintl phase.

mation to the crystal potential was made. We find the system to show a semimetallic band structure with a hole pocket around Γ and an electron pocket along Δ . The band structure is qualitatively similar to that of the diamond-type IV-IV tetrahedrally bonded semiconductors with a substantial reduction in the main band gaps (in particular the $\Gamma_{25'}-X_1$ gap which becomes negative). We use our resulting band structure and density of states to suggest tentative models for the observed anomalies in the transport properties as well as to predict the (yet unknown) features of the optical and x-ray photo-emission spectra. A detailed study of the variational crystal wave function and charge density is carried out to gain some understanding of the bonding mechanisms in the system. We find that the Li-Al bonds are weakly covalent with a stronger polarization towards the Al sites, indicating a partial ionic character, while the Al-Al bonds are essentially metallic. The Li-Li contacts are found to be nonbonding and hence intrinsic defects can presumably form on this sublattice.

II. APPROACH TO SELF-CONSISTENCY

We wish to solve, for the LiAl system, the all-electron local-density one-particle equation^{13,14} given by

$$\left\{-\frac{1}{2}\nabla^2 + V(\rho(\vec{r}))\right\}\psi_j(\vec{k}, \vec{r}) = \epsilon_j(\vec{k})\psi_j(\vec{k}, \vec{r}), \quad (1)$$

where $\psi_j(\vec{k}, \vec{r})$ and $\epsilon_j(\vec{k})$ denote the crystal wave function and the one-electron band eigenvalues, respectively, for band index j and Brillouin-zone (BZ) wave vector \vec{k} . The crystal potential is given by¹³⁻¹⁵

$$V(\rho(\vec{r})) = V_{\text{SRC}}(\rho(\vec{r})) + V_{\text{LRC}}(\vec{r}) + V_{\text{xc}}(\rho(\vec{r})), \quad (2)$$

where the electrostatic part is partitioned for convenience into short- and long-range Coulomb parts V_{SRC} and V_{LRC} , respectively. The former constitutes the potential due to the (inhomogeneous) electronic charge density $\rho(\vec{r})$ and the bare nuclear charges $Z_{\alpha,m}$, compensated by the net ionic charge $Q_{\alpha,m}$ at lattice site α in unit cell m :

$$V_{\text{SRC}}(\rho(\vec{r})) = \int \frac{\rho(\vec{r}')}{|\vec{r} - \vec{r}'|} d\vec{r}' - \sum_{m,\alpha} \frac{Z_{\alpha,m} + Q_{\alpha,m}}{|\vec{r} - \vec{R}_m - \vec{d}_\alpha|}, \quad (3)$$

while the electrostatic field due to a lattice of charges $\pm Q_{\alpha,m}$ yields the long-range Coulomb potential $V_{\text{LRC}}(\vec{r})$, constructed using Ewald techniques.¹⁷ The local exchange and correlation potential $V_{\text{xc}}(\rho(\vec{r}))$ is

$$V_{\text{xc}}(\rho(\vec{r})) = V_x(\rho(\vec{r})) + V_c(\rho(\vec{r})), \quad (4)$$

where the exchange part V_x is given by the $\rho(\vec{r})^{1/3}$

term¹⁴ (with exchange coefficient of $\alpha = \frac{2}{3}$) while the nongradient correlation potential V_c is given by Singwi *et al.*¹⁸ Equation (1) is to be solved self-consistently by iteratively constructing the potential from the all-electron variational crystal density

$$\rho_{\text{cry}}(\vec{r}) = \int_{\text{OBZ}} \sum_j^{\text{occ}} n_j(\vec{k}) |\psi_j(\vec{k}, \vec{r})|^2 d\vec{k}, \quad (5)$$

with no shape approximations (e.g., muffin tin, spherical cellular, etc.) to the potential. Here $n_j(\vec{k})$ denotes the Fermi occupation numbers and the summation and integration are performed over the occupied BZ (OBZ). We have previously developed a method^{15,16} capable of treating self-consistently such general crystal potentials within nonlinearly-optimized numerical linear-combination-of-atomic-orbitals (LCAO) basis sets. We will hence indicate here only the details of the method pertaining to this study and refer the reader to the previous reports for more general details.

Our starting point is to provide a model for the crystal charge density that would enable an efficient initiation of the crystal potential and self-consistency (SC) calculation. We use the population-dependent superposition model in which one first solves self-consistently the *single-site* LDF equation [Eq. (1)] for the individual Li and Al species [assuming a set of central field (n, l) orbital occupation numbers f_{nl}^α and net charges Q_α], and then superposes the resulting SC single-site densities $\rho_\alpha(r, \{f_{nl}^\alpha, Q_\alpha\})$ to yield the model density

$$\rho_{\text{sup}}(\vec{r}, \{f_{nl}^\alpha, Q_\alpha\}) = \sum_{m,\alpha} \rho_\alpha(\vec{r} - \vec{R}_m - \vec{d}_\alpha, \{f_{nl}^\alpha, Q_\alpha\}). \quad (6)$$

Here the single-site orbital occupation numbers form a quasicontinuous set (subject to the exclusion principle) that covers the ground as well as excited (neutral or ionic) configurations of the Li $1s, 2s, 2p$ and Al $1s, 2s, 2p, 3s, 3p, 3d$ orbitals. Different choices of these occupation numbers in a self-consistent single-site calculation can produce substantial nonlinear variations in $\rho_\alpha(r)$ due to the changes in screening of the occupied levels (orbital relaxation) as well as due to fractional population of formerly virtual orbitals. These orbital population numbers are subsequently used as variational parameters in the course of the SC iteration for the *crystalline* calculation, enabling thereby to naturally account for a large part of the charge redistribution in the solid relative to the ground state of its constituent atoms. Note however, that although nonspherical site components are present in $\rho_{\text{sup}}(\vec{r})$ (spherical muffin-tin averaging is avoided), it is still plausible that the full site anisotropy present in the *variational* density $\rho_{\text{cry}}(\vec{r})$ [Eq. (5)] is not reproduced by a nonlinear optimized

superposition model which involves only a limited number of expansion centers (i.e., existing atoms). We treat this part of the density, i.e.,

$$\Delta\rho(r) = \rho_{\text{cry}}(r) - \rho_{\text{sup}}(r, \{f_{ni}^\alpha, Q^\alpha\}), \quad (7)$$

later. The superposition density [Eq. (6)] is used to calculate the various components of the crystal potential [Eqs. (2)–(4)] directly in real space by performing the relevant lattice summations to within a cutoff distance of 27 a.u. (relative error of $1:10^8$).

The crystal wave functions $\psi_j(\vec{k}, \vec{r})$ are expanded in standard form in terms of Bloch functions $\Phi_{\mu,\alpha}(\vec{k}, \vec{r})$ constructed from the basis orbitals $\chi_{\mu,\alpha}(\vec{r})$ of orbital index μ and atomic species α . We chose as $\chi_{\mu,\alpha}(\vec{r})$ the accurate SC numerical solutions of the single-site LDF one-particle equation corresponding to the occupation numbers $\{f_{\mu}^\alpha, Q^\alpha\}$ discussed before. These solutions are not constrained to be fitted to simple analytical forms (e.g., Gaussians or Slater orbitals) and possess the appropriate nodal behavior and cusps. We chose an extended basis set composed of Li 1s, 2s, 2p and Al 1s, 2s, 2p, 3s, 3p, and 3d orbitals.¹⁹ The main advantage of this type of basis set lies in the considerable nonlinear variational flexibility offered by its generating algorithm (i.e., by changing the physically transparent parameters of the problem, the single-site orbital occupation numbers, desired radial distortions are obtained) and by its close correspondence to the crystal potential at hand (e.g., a choice of atomic Hartree-Fock rather than LDF orbitals to be used with a local-density crystal potential²⁰ produces larger deviations $\Delta\rho(\vec{r})$ [Eq. (7)] from self-consistency unless very sizeable basis sets are used). Our previous studies on diamond,²¹ boron nitride,²² LiF,²⁰ and TiS₂,²³ using these basis sets have indicated a rapid convergence of the variational density and band eigenvalues with respect to the basis-set size (e.g., a numerical basis set consisting of 19 Bloch functions produced in LiF virtually the same results²⁰ that were obtained with 54 Gaussian Bloch functions²⁴). We find that the inclusion of Al 3d orbitals (lying in the atomic LDF model at about 2.7 eV above the Al 3p level) is essential to maintain reasonable accuracy in the band structure for both the upper portion of the occupied bands and the unoccupied bands. A non-self-consistent solution using a crystal potential generated from ground-state atomic densities and including Al 3d basis functions showed shifts of 0.29 and 0.31 eV in the $X_{1,v}$ and $X_{4,v}$ valence-band states, respectively, and shifts of -0.04, 0.49, and 0.79 eV for the conduction states $X_{1,c}$, $X_{3,c}$, and $\Gamma_{25,c}$, respectively, relative to a calculation with the same potential but without the 3d orbitals. Addition of

more basis functions (e.g., Slater-type *s*, *p* functions for Li and Al) produced negligible changes (≤ 0.02 eV) in the band structure for energies lower than 10 eV above the Fermi energy ϵ_F and was consequently ignored. Figure 2 shows a few of the Bloch functions $\Phi_{\mu,\alpha}(0, \vec{r})$ for the LiAl structure, at the zone center. Note that the Li 2s and 2p Bloch functions are long ranged and have substantial magnitudes at the Al site. Thus, it is clear that there is no simple way of partitioning space into Li and Al charge density "domains."

The matrix elements of the crystal potential $V(\rho(\vec{r}))$ within the Bloch basis $\Phi_{\mu,\alpha}(\vec{k}, \vec{r})$ are calculated here in direct space using the three-dimensional Diophantine integration scheme.^{25,26} The well-known difficulties associated with evaluating the many-center Coulomb and exchange integrals appearing in other real-space techniques²⁷ are completely avoided as are the problems involved with the slowly convergent Fourier representation of the all-electron wave functions and potential, encountered in reciprocal-space techniques.²⁸ Convergence to within 0.02 eV in the band eigenvalues below $\epsilon_F + 10$ eV is obtained for 700 and 550 points per Al and Li sites, respectively, and an additional 1500 points in the interatomic space (i.e., a total of 4000 points per unit cell). Note, however, that due to the long range of the LDF Bloch functions, the convergence of the Hamiltonian and over-

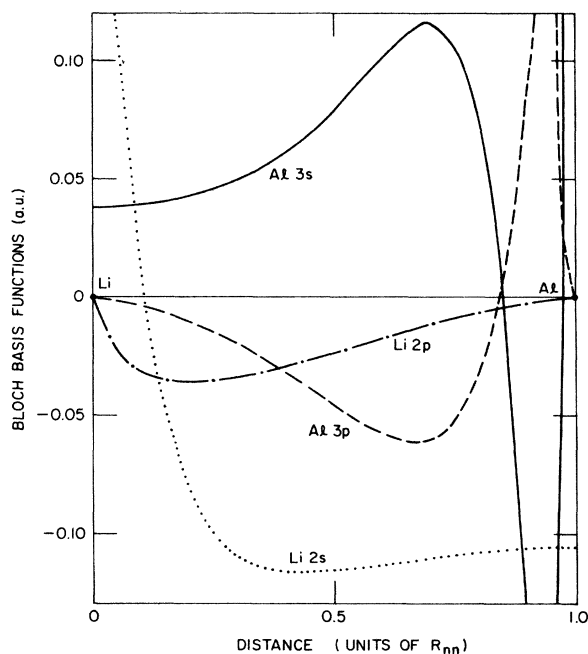


FIG. 2. Bloch function for the LiAl structure at Γ along the Li-Al bond direction. The single-site orbitals are normalized to unity and R_{nn} denotes the nearest-neighbor distance.

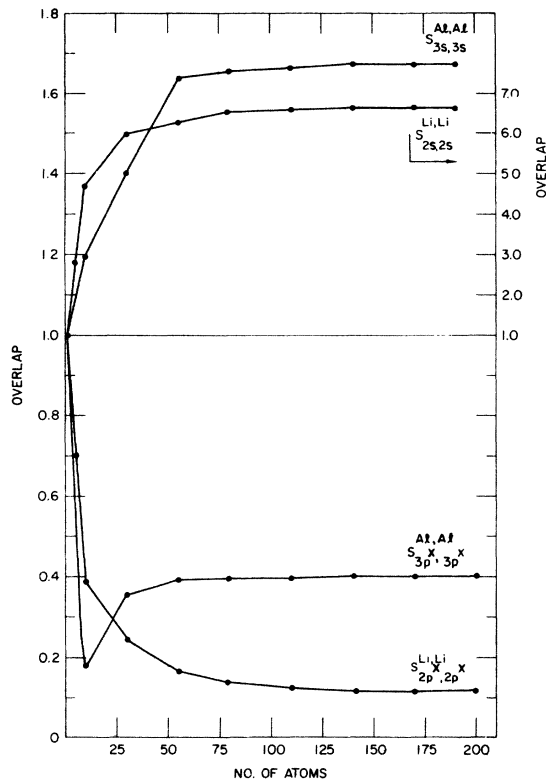


FIG. 3. Convergence of the overlap matrix elements between the Bloch functions at Γ , as a function of the number of sites included in the Bloch sums.

lap matrix elements with respect to the range of the Bloch sums, is rather slow. Figure 3 shows the dependence of the overlap matrix elements at the zone center on the number of sites included in the Bloch sums [here the individual basis orbitals $\chi_{\mu\alpha}(\vec{r})$ are orthonormal at each site and consequently the Bloch functions $\Phi_{\mu\alpha}(\vec{k}, \vec{r})$ are not normalized to unity]. It is seen that these elements are stabilized to within 1% of their converged value only after some 130 atoms around the origin are included. In particular, substantial changes in these overlap elements occur for clusters containing less than 30 atoms around the origin site. Although it is possible to accelerate this convergence rate by further localizing the basis functions,²⁹ our previous studies²¹ have indicated that extreme care has to be practiced when the stability of the band structure (rather than the total energy) is used as the only criteria for the orbital localization scheme employed. In particular, we find²¹ that although the diamond band structure can be reproduced fairly accurately (~ 0.04 eV) over a relatively wide energy range (valence plus first conduction band) by using truncated orbitals, the bonding mechanism and cohesive properties (that are sen-

sitive to the details of the orbital tails) are altered dramatically (e.g., 30% reduction in cohesive energy). We have hence avoided any localization scheme other than that offered by the variation of the single-site occupation $\{f_{n\beta}^{\alpha}\}$ (that serves to occasionally contract orbitals due to changes in the orbital screening) which, in turn, is dictated by the self-consistency requirement in the solid.

At this initial step in the calculation one desires to find a set of single-site occupation numbers and net charges $\{f_{n\beta}^{\alpha}, Q_{\alpha}\}$ that when used to construct both the basis Bloch functions and the superposition potential would yield a variational density $\rho_{\text{cry}}(\vec{r})$ which minimizes the non-self-consistency deviation $\Delta\rho(\vec{r})$ [Eq. (7)]. Such a procedure accounts for those charge-redistribution effects involved in bonding in the solid that are amenable to description by predominantly intra-atomic single-site orbital relaxation effects. Although such a minimization of $\Delta\rho(\vec{r})$ can be carried out directly (e.g., using a least-squares criteria^{15,16}), it seems advantageous to consider here some limiting cases first. The diamond-type tetrahedral site coordination present in LiAl has led to the suggestion^{1,30} that the atoms involved in bonding would maintain an effective sp^3 outer shell hybrid (e.g., Li $2s^x 2p^{3x}$ and Al $3s^y 3p^{3y}$) characteristic of the IV-IV and III-V systems. Such an arrangement can be realized in the *ionic* limit by transferring the Li 2s electron into the Al 3p shell accompanied by an *s-p* intra-atomic promotion in Al ($x=0, y=1$), while in the *neutral* atom limit this is established in the configuration $x=\frac{1}{4}, y=\frac{3}{4}$. [In the general case where the fractional charges are $+Q$ on Li and $-Q$ on Al, the configuration would be $X=\frac{1}{4}(1-Q)$ and $y=\frac{1}{4}(3+Q)$.] Hence, it seems interesting to first try these limiting configurations. Figure 4 shows the band structure along the Γ -X direction obtained with (a) the ground-state Li⁰ $1s^2 2s^1 2p^0$, Al⁰ $1s^2 2s^2 2p^6 3s^2 3p^1 3d^0$ configuration; (b) the neutral excited sp^3 configuration $Q_{\text{Li}}=Q_{\text{Al}}=0, x=\frac{1}{4}, y=\frac{3}{4}$; and (c) the ionic sp^3 configuration $Q_{\text{Li}}=-Q_{\text{Al}}=1; x=0, y=1$. The energies of some of the high-symmetry points in the BZ and the principal gaps are given in Table I. It is seen that the principle change in the band structure relative to the neutral ground-state configuration is a rigid downwards shift of the bottom of the bands of about 4.9 eV in the excited sp^3 model and 2.8 eV in the ionic model while the \vec{k} -dependent shifts are almost an order of magnitude smaller, the energy separations in the occupied bands are generally less sensitive than the corresponding valence to conduction gaps.

We find that the deviation from self-consistency is about the same in all three limiting cases, the excited neutral sp^3 configuration choice being only

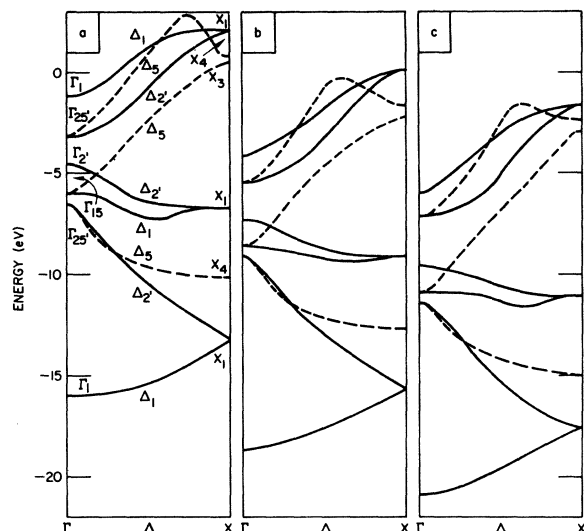


FIG. 4. Band structure along the Γ -X direction obtained from the three limiting configurations: (a) $\text{Li}^0 1s^2 2s^1 2p^0$, $\text{Al}^0 1s^2 2s^2 2p^6 3s^2 3p^1 3d^0$; (b) $\text{Li}^+ 1s^2 2s^0 2p^0$, $\text{Al}^- 1s^2 2s^2 2p^6 3s^1 3p^3 3d^0$; (c) $\text{Li}^0 1s^2 2s^{0.25} 2p^{0.75}$, $\text{Al}^0 1s^2 2s^2 2p^6 3s^{0.75} 3p^{2.25} 3d^0$. Dashed lines indicate doubly degenerate representations.

marginally better than the ionic sp^3 and the ground-state configuration (0.18% of the electrons are misplaced by the latter model). This suggests that the choice of basis orbitals that “match” the choice of the crystal potential (i.e., both are generated from SC solutions to LDF single-site equations) has exhausted the possible degree of self-consistency that can be obtained within a *superposition* model. (This is not surprising since the long range of the Li 2s and 2p Bloch orbitals even in the ground-state configuration, cf. Fig. 2, can simulate Li to

TABLE I. Energy (in eV) of high-symmetry points in the BZ as obtained by the three limiting superposition models, relative to the corresponding vacuum levels.

Level	Ground	Ionic sp^3	Excited sp^3
Γ_1	-15.95	-18.73	-20.81
$\Gamma_{25'}$	-6.49	-9.04	-11.40
Γ_{15}	-6.05	-8.61	-10.97
$\Gamma_{2'}$	-4.52	-7.33	-9.56
$\Gamma_{25''}$	-3.15	-5.56	-7.18
X_1	-13.16	-15.74	-18.02
X_4	-10.10	-12.74	-15.10
X_1	-6.74	-9.16	-11.05
$L_{2'}$	-14.58	-17.18	-19.23
L_1	-12.58	-15.16	-17.15
L_3	-8.02	-10.49	-12.67
L_3	-6.44	-8.94	-10.71
L_1	-5.96	-8.33	-10.53

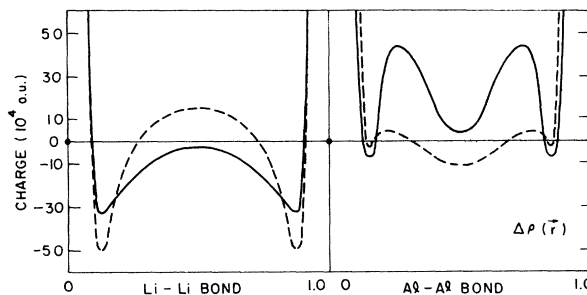


FIG. 5. Differences in crystal charge densities obtained with the neutral ground-state model relative to the excited neutral model $\rho_{\text{cry}}^0(\vec{r}) - \rho_{\text{cry}}^*(\vec{r})$ (full lines) and the corresponding difference $\rho_{\text{cry}}^0(\vec{r}) - \rho_{\text{cry}}^\pm(\vec{r})$ relative to the excited ionic model (dashed lines), along the Li-Li and Al-Al bond directions.

Al charge transfer as well as the s to p promotion, solely by wave-function overlap rather than by actual exchange of point charges.²⁰) This, however, does not imply that full self-consistency has been reached by any of these starting configurations: the significant changes in the one-electron energies obtained in these three models (as much as 4.9 eV in the position of the Fermi level relative to the vacuum and 0.6 eV in the interband transition energies) suggests that relatively small changes in the overall superposition density produce not only sizable rigid shifts in the band structure but the even smaller changes in the site anisotropies yield non-negligible changes in the dispersion itself. Clearly, these small changes in the residual $\Delta\rho(\vec{r})$ cannot be satisfactorily annihilated by a superposition model.

Figure 5 shows that difference in the crystal densities $\rho_{\text{cry}}(\vec{r})$ obtained with the ground-state configuration relative to the neutral-excited configuration $\rho_{\text{cry}}^0(\vec{r}) - \rho_{\text{cry}}^*(\vec{r})$, as well as the difference $\rho_{\text{cry}}^0(\vec{r}) - \rho_{\text{cry}}^\pm(\vec{r})$ between the ground and the excited ionic configuration. In each case, the BZ integral in Eq. (5) has been replaced by a weighted sum over 24 \vec{k} vectors³¹ in the irreducible section of the BZ, where the weights are chosen according to the nearest-volume criteria for points well under the Fermi surface and according to the fraction of occupied volume for points near the surface.³² It is seen that both excited configurations act to delete some charge density from the atomic “core” regions and place it along the bonds, these changes being less pronounced in the bond centers than in the bond edges. Clearly, only minor s to p promotion seems to occur in the system relative to the ground-state configuration and a previously speculated^{1,30} genuine ionicity of the bond cannot be inferred. A more complete search in the configuration space of $\{f_{ni}^\alpha, Q_\alpha\}$ has similarly failed to reveal any pronounced minima in the deviation

from self-consistency $\int |\Delta\rho(\vec{r})| d\vec{r}$.

To include in our treatment the full-site anisotropies exhibited by $\rho_{\text{cry}}(\vec{r})$, we have to go beyond the optimized superposition model. This is conveniently done by Fourier analyzing $\Delta\rho(\vec{r})$ [Eq. (7)] and solving the associated Poisson equation in reciprocal space.^{15,16} Since the major charge-redistribution effects are already exhibited by the superposition density, $\Delta\rho(\vec{r})$ is a smooth function and gives rise to a rapidly convergent Fourier representation.¹⁵ The interelectronic Coulomb potential due to $\Delta\rho(\vec{r})$ is then given by

$$\Delta V(\vec{r}) = \sum_{\vec{K}_s \neq 0} -\frac{4\pi}{|\vec{K}_s|^2} \Delta\rho(\vec{K}_s) e^{i\vec{K}_s \cdot \vec{r}}, \quad (8)$$

where the first 12 symmetrized plane waves $|\vec{K}_s\rangle$ are used. $\Delta V(\vec{r})$ is then added to $V_{\text{SRC}} + V_{\text{LRC}}$ obtained in the last iteration in the superposition model and to the modified exchange-correlation potential $V_{\text{xc}}[\rho_{\text{sup}}(\vec{r}) + \Delta\rho(\vec{r})]$, to yield the updated crystal potential. The calculation is repeated so as to reduce the differences $\Delta\rho(\vec{r})$ between successive iterations. As the end of the SC cycle (eight iterations), the "misplaced" charge $\int |\Delta\rho(\vec{r})| d\vec{r}$ is only 0.03% of the total unit cell charge and the band eigenvalues are stabilized to within 0.03 eV. This model avoids the partitioning of the crystal density into contributions from atomic sites and leads to a unique SC density.

III. RESULTS

A. Band structure and density of states

The self-consistent band structure of LiAl in the exchange and correlation local density model is depicted in Fig. 6 where standard labels of the face-centered-cubic BZ are used. The band structure has been fitted to a set of 12 fcc symmetrized plane waves using 24 calculated \vec{k} points along the faces of the irreducible section of the BZ and an additional 30 \vec{k} points inside the irreducible BZ. The fitted bands were then used to compute the density of states and Fermi energy (Fig. 7) using the analytic tetrahedron scheme^{33,34} (6656 microtetrahedra were used). The energy separations between some of the high-symmetry levels in the occupied and unoccupied bands are given in Table II.

It is seen from Fig. 6 that LiAl is a semimetal with a hole pocket around Γ and an electron pocket along Γ -X (close X). There is a striking similarity between the band structure of LiAl and that calculated for the IV-IV systems: diamond,³⁵ silicon,³⁶⁻³⁹ germanium,³⁷⁻³⁹ and α -Sn.³⁷⁻⁴⁰ The indirect $\Gamma_{25'} - X_1$ gaps^{38,39} decrease from the value of 5.48 eV in diamond to 1.13 eV in Si, 0.96 eV in Ge; our calculated value for LiAl is -0.18 eV. Similarly, the direct $\Gamma_{25'} - \Gamma_{15}$ (E'_0) separation is 7.3

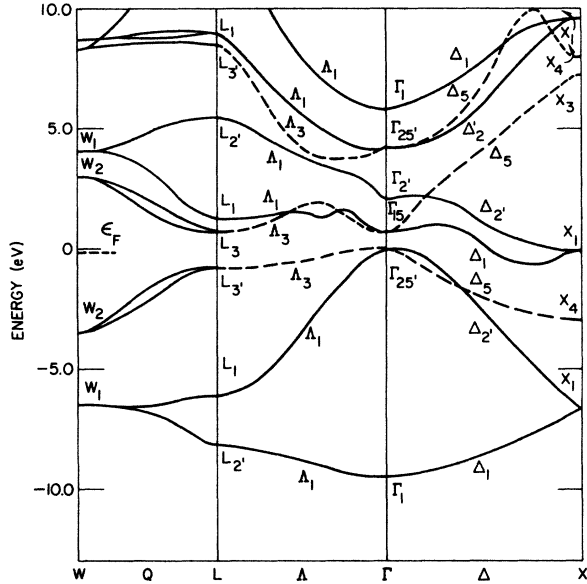


FIG. 6. Self-consistent band structure of LiAl in the exchange and correlation model. Dots on the abscissa indicate calculated points. Dashed lines indicate doubly degenerate representations. Lattice constant, 6.333 Å (Refs. 1 and 10).

eV in diamond, 3.35 eV in Si, 3.19 eV in Si, and close to zero in α -Sn,^{37,39,40} as compared to our calculated value of 0.47 eV in LiAl. Similar trends are observed in the $X_4 - X_1$ (E_{2A}) separation^{38,39} which is 12.2 eV in diamond, 4.4 eV in Si, 4.3 eV in Ge, about 3.7 eV in α -Sn,³⁸ while in our calculation for LiAl yields 3.5 eV. It is noted, however, that the differences between LDF band eigenvalues of occupied and unoccupied states do not correspond in general to the elementary excitations observed spectroscopically and that self-energy corrections

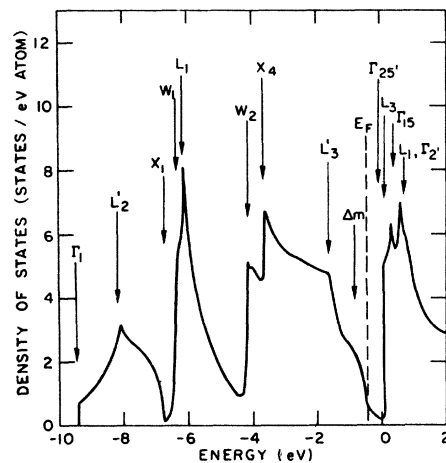


FIG. 7. Density of state of LiAl. The arrows point to high-symmetry points in the BZ.

TABLE II. Energy separation (in eV) for various valence and conduction states in LiAl. Δ_m indicates the minimum point in the lowest Γ - Δ - X conduction band at $(2\pi/a)(0.8, 0, 0)$.

Valence-conduction		Valence-valence		Conduction-conduction	
$\Gamma_{25'} \rightarrow \Gamma_2$	1.83	$\Gamma_1 - \Gamma_{25'}$	9.44	$\Gamma_{25'} \rightarrow X_1$	-0.18
$L_3 \rightarrow L_1$	2.11	$X_1 - X_4$	2.95	$X_1 - X_4$	7.08
$X_4 \rightarrow X_1$	3.48	$L_2 - L_1$	2.04	$\Gamma_{25'} - \Delta_m$	-0.53
$\Gamma_{25'} \rightarrow \Gamma_{15}$	0.47	$L_1 - L_3$	4.61	$\Gamma_{15} - \Gamma_{2'}$	1.35
$L_3 \rightarrow L_3$	1.49			$\Gamma_{25'} - \Gamma_{25'}$	3.40

have to be applied.^{20,41} In systems where some spatial localization in the initial or final states occurs, the self-interaction effects (i.e., the residual of the noncancellation between Coulomb and exchange-correlation self-interaction) as well as relaxation and polarization effects can be significant.²⁰

The ordering of the two lowest conduction bands at Γ varies along this series: calculations for diamond²¹ and silicon^{36,39} place the p -like Γ_{15} state lower than the s -like $\Gamma_{2'}$ state (as is also the case in LiAl), while the order is reversed in Ge and α -Sn.^{37,39} Similarly, while in diamond^{21,42} and in LiAl the two lowest conduction states at L are L_3 and L_1 , their order appears to be reversed in^{36,37} Si and ³⁷ Ge. The width of the occupied portion of the bands decrease from about 22 eV in diamond^{21,42} to 15 eV in Si, 13 eV in Ge, whereas our calculated value for LiAl is 9.4 eV. This tendency towards metallization as one goes from diamond towards LiAl parallels the increase in energy cost to provide an s to p promotion necessary to form an sp^3 hybrid.⁴³ Furthermore, the covalent binding energy which is required to compensate for the valence promotion energy decreases along this series. The covalent-bond energy parameter⁴⁴ which is related to the interaction matrix element between nearest-neighbor hybrid orbitals $\beta = -\langle \varphi_a | H | \varphi_b \rangle / (1 - \langle \varphi_a | \varphi_b \rangle^2)$, and provides a measure of the strength of the covalent bond, decreases monotonically as one goes from diamond ($\beta = 6.1$ eV) to Si ($\beta = 2.2$ eV), Ge ($\beta = 2.15$ eV), and finally to α -Sn ($\beta = 1.76$ eV). The bond-orbital argument for correlating β with the bond length⁴⁴ places LiAl in that series between Ge and α -Sn, but somewhat closer to the latter. Clearly, the simplified arguments cannot be pursued in greater detail due to the rather involved electronic structure differences in these compounds (e.g., variation in spin-orbit contributions and d -orbital hybridization); they do seem to provide, however, a qualitative understanding of the trends in the series and to correlate with some detailed quantum-mechanical studies on the covalent bonding in these systems.⁴⁵

In order to see whether the semimetallic ordering of the energy levels in LiAl is peculiar to the situation where the bonds are "strained," we have repeated the band-structure calculation varying the lattice parameter a . Using $a = 12.48$ a.u. (which yields bond lengths like those in metallic Li), $a = 13.26$ a.u. (yielding bond lengths like in metallic Al), and three additional equispaced points in between, we find that the X_1 conduction state and the minima along the Δ direction, is lower than the $\Gamma_{25'}$ (but higher than the X_4 state) in the entire lattice-parameter range, yielding a semimetallic character. The $\Gamma_{25'} - X_1$ energy separation increases with increase of the lattice parameter from 0.18 eV (at $a = 12.04$ a.u.) to 0.25 eV (for $a = 13.26$ eV). We similarly find that when the lattice constant is reduced from its equilibrium zero-pressure value for LiAl (12.04 a.u.), the $\Gamma_{25'} - X_1$ gap is reduced but is not closed up until a is smaller than 11.5 a.u. [Note that in a diamond-type empty lattice the $\Gamma_{25'}$ state is higher than the X_1 state by $(1/2m)(2\pi/a)^2$ and that the covalent interactions present in the actual crystal, act to reduce this gap.] This suggests that LiAl would eventually become a semiconductor under pressure. Interestingly, we find that the $\Gamma_{2'}$ state interchanges its position with the Γ_{15} state for lattice parameters larger than 13 a.u. (the antibonding s -type $\Gamma_{2'}$ state has a negative pressure derivative while the p -type Γ_{15} state has a small positive pressure derivative, similar to the situation found in diamond²¹) yielding the level order characteristic of Ge.

A preliminary non-self-consistent calculation of the band structure of LiAl was previously performed by Switendick⁴⁶ using the augmented-plane-wave (APW) method in the muffin-tin approximation. His results are in qualitative agreement with ours: the X_1 conduction level lies some 0.5 eV below the $\Gamma_{25'}$ level and the $\Gamma_1 - \Gamma_{25}$ valence band width is about 9.3 eV. Some differences seem to occur in the conduction level ordering (L_1 and L_3) and similarly the lowest conduction band along Δ appears to decrease monotonically away from Γ , in contrast with our results in which a minimum is

found. If the Fermi energy is placed between the $\Gamma_{25'}$ and the X_1 levels, as is the case in our calculation, the APW results would indicate electrons at X and holes at Γ , similar to the situation found in the present calculation.

The density-of-states curve (Fig. 7) is again qualitatively similar to that of the IV-IV compounds.^{37,39} Three main peaks are found in the valence bands: the lowest peak at 8.1 eV below ϵ_F originating from an M_1 singularity at L'_2 , then the M_2 -type peak at 6.1 eV below ϵ_F due to states near L_1 , and finally a split and broad peak due to states along Σ - W - X in the third valence band between 2 and 4 eV. The density of states near the Fermi level decreases very steeply due to the pronounced slope of the bands below $\Gamma_{25'}$, and reaches a low value of about 0.05 states/(eV atom) at ϵ_F . This is about 20% of the value calculated for metallic Al,^{47,48} and about 10% of the value obtained for metallic Li.^{49,50} Due to the occurrence of a constant concentration of vacancies in LiAl even for stoichiometric samples,^{3,10} it is possible that the Fermi level in real samples lies somewhat lower in energy where the density of states is enhanced considerably. The width of the occupied band in LiAl (9.4 eV) is intermediate between that calculated for metallic Li (3.5 eV)^{49,50} and metallic Al (11.1 eV)⁴⁶ and similarly the Fermi-level position (relative to the vacuum) (6.5 eV) is close to the average of the values obtained for Al (8.5 eV)⁴⁸ and Li (3.9 eV).⁵⁰

B. Knight shifts and susceptibilities

The measurements of the Knight shift of Schone and Knight³ have indicated almost zero shift (within experimental accuracy) for Li⁷ (reference compound LiCl) and a reduction of about 93% in the Al²⁷ Knight shift relative to metallic Al. Due to the unavailability of accurate data on the paramagnetic susceptibilities of LiAl and Al, only rough estimates can be made to understand the origin of this dramatic lowering. The Knight shift K_α at site α is proportional to the Pauli spin susceptibility χ_P and the expectation value of the square of the Fermi-level wave function at nucleus α .⁵¹ The ratio between the Al²⁷ shift in LiAl and in metallic Al, $K_{\text{LiAl}}/K_{\text{Al}}$ (observed values 0.06 ± 0.02)³ is given by the product of the susceptibility ratio $\chi_{\text{LiAl}}/\chi_{\text{Al}}$ and the contact s -charge densities ratio $\langle \psi_{\text{Al}}^2(0) \rangle_{\text{LiAl}} / \langle \psi_{\text{Al}}^2(0) \rangle_{\text{Al}}$ at the Al sites, if exchange-polarization contributions of p and d electrons are neglected. [Bennett, Watson, and Carter⁵¹ have estimated the contribution of the core-polarization effects for p electrons in metals and found them to be small (and positive) for shells with principle quantum numbers smaller or equal to 3.]

Several estimates exist for the contact s density in pure metals (obtained mainly from Knight-shift and heat-capacity data); expressed as a fraction of the calculated atomic $3s$ density in isolated Al, this value is about 0.25 in metallic Al.⁵¹ We have calculated the contact s density at the Al site in LiAl from the three bands which cross ϵ_F . Normalized to the atomic $3s$ contact density (obtained from a SC solution to the LDF atomic equation), this value is 0.08, i.e., some 30% of the value in the pure metal (the correspondingly calculated value for Li in LiAl is 0.002). Using the measured Knight-shift ratio, this predicts a susceptibility ratio of $\chi_{\text{LiAl}}/\chi_{\text{Al}} \approx 0.2$. Thus, the small observed Knight shift appears to arise from the combined effects of the reduction in Al s character and a decrease in susceptibility in going from the metal to the LiAl compound. Using the experimental estimate for the susceptibility of metallic Al [$\sim 1.1 \times 10^{-6}$ cgs mass units (Ref. 52)], one arrives at an estimate of $\sim 0.2 \times 10^{-6}$ cgs mass units for the Pauli susceptibility in LiAl, a value close to the value deduced by Yao¹² from measurements of the total susceptibility in LiAl subject to diamagnetic core corrections.⁵³ The ratio of the susceptibilities $\chi_{\text{LiAl}}/\chi_{\text{Al}} \approx 0.2$ is similarly close to the ratio between the density of states at ϵ_F , $D(\epsilon_F)_{\text{LiAl}}/D(\epsilon_F)_{\text{Al}} \sim 0.23$ [using $D(\epsilon_F)_{\text{Al}} = 0.22$ state/(eV atom) from Ref. 46; similar results are given by Snow and by Faulkner⁴⁸]. This reduction in spin susceptibility and density of states at ϵ_F , is consistent with the fact that contrary to the situation in the pure metals, no conduction electron contribution to the T_1 relaxation time was detected in magnetic resonance measurements in LiAl.^{4,5}

Electrical-resistivity measurements in LiAl in the 77–300 °K region¹⁰ have indicated poor metallic conductivity (27 $\mu\Omega$ cm for LiAl compared with 9.3 $\mu\Omega$ cm and 2.7 $\mu\Omega$ cm for Li and Al, respectively, at 295 °K).⁵⁴ The conductivity seems to be predominantly electronic, since nuclear magnetic measurements on the Li diffusivity⁴ indicate low ionic conduction [$\sim 1(\Omega \text{ m})^{-1}$ at 300 °K]. The resistivity was nearly linear with temperature near 300 °K but showed a pronounced increase in slope at lower temperatures. It would seem difficult at this stage to assess the possible significance of electron-phonon versus semimetallic electron-hole contributions to the resistivity before more data is available on the low-temperature behavior as well as on the nature of the residual resistivity in this defect-rich material.

Studies on the Li concentration dependence of the electrical resistivity have indicated that the room-temperature resistivity rises sharply for excess Li samples (from 21 $\mu\Omega$ cm at 50% Li to 60 $\mu\Omega$ cm at 52% Li). Similar studies by Yao¹² on the mag-

netic susceptibility as a function of Li concentration show an abrupt decrease in χ from 50% to 52.5% Li. Nuclear-magnetic-resonance experiments on the Li⁷ dipolar line narrowing with temperature⁵ indicate that samples of 50% and 52% Li contain a concentration of about 2.4% and 0.3% vacancies, respectively, and that this concentration is most temperature independent. Hence, it is possible that the stoichiometric LiAl crystals possess less than the nominal number of 32 electrons per cell and hence have their Fermi energy considerably below the $\Gamma_{25'}$ level, in the metallic region (cf. Fig. 6). As the Li content increases to 52%, almost all the bands below our calculated Fermi energy for the ideal crystal become occupied and hence the Fermi-surface area (and to a lesser degree the density of states at ϵ_F) decrease rather abruptly in going towards the "semimetallic" region of the bands. This lowers the susceptibility and increases the resistivity and appears to be consistent with the fact that both the resistivity¹⁰ and the susceptibility¹² are much less sensitive to Li concentration in 48%–50% region (e.g., a change in resistivity from 18 to 21 $\mu\Omega$ cm). According to our model, this leaves the system still in a metallic region where only changes in the nature of the scattering centers (i.e., Li vacancies) govern the transport properties.

Preliminary measurements of the differential resistivity of LiAl in the 80–150 °K region, have been reported by Cristea *et al.*¹⁰ Their measurements (carried out on Li-deficient samples) indicate, that upon cooling, a sharp rise of the temperature derivative of the resistivity occurs around 105 °K, followed by a decay at lower temperatures. This peak in the differential resistivity seems to decrease in amplitude and shift to lower temperatures when the Li content of the sample increases. Although some detailed electron-diffraction studies are needed to establish whether a structural change accompanies the discontinuity in the differential resistivity, it is interesting to speculate on its possible origin. We note that a very similar behavior of the differential resistivity with temperature and doping occurs in some of the metal dichalcogenides (e.g., TiSe₂)⁵⁵ where it was identified with a superlattice transition of the variety of charge-density wave instabilities, presumably induced by coupling of electrons and holes that exist in the semimetallic pockets around *L* and Γ , respectively (separated by a zone-boundary wave vector). Thus, it seems possible that a Fermi-surface nesting or volume effect (induced by two parallel bands crossing ϵ_F , such as that evident for the Γ -*X* bands in Fig. 6) together with the corresponding electron-phonon matrix element would couple the electron-hole pockets in LiAl and intro-

duce a gap opening (viz., increase in resistivity) and a structural change.

C. Charge density and bonding

The bonding mechanism in LiAl has been the subject of speculation.^{1,30,56} The tetrahedral site symmetry of its constituent atoms has led Hückel³⁰ and Zintl¹ to suggest an sp^3 bonding in which a Li atom transfers its valence electron to the Al atom to yield an Li⁺Al⁻ structure where the Al have four valence electrons just as carbon and silicon. However, application of Pauling's bond-number-bond-length relation,⁵⁷ which holds remarkably well for all sp^3 bonded compounds, leads to bond lengths in LiAl that are about 6% too short. Similarly, local-density total energy calculations for the Li⁰, Li⁺, Al⁰ and Al⁻ isolated species indicate that about 7–9 eV (depending on the various assumptions used for the exchange and correlation potential) are needed to generate the required valence hybrids for each LiAl pair. This leaves a large energy barrier to be compensated by the crystal cohesion (cf. the net cohesion of the pure metals is 1.63 and 3.39 eV/atom for Li and Al, respectively⁵⁸).

Our band calculation indicates that LiAl would have been a narrow gap semiconductor if it were not for the small overlap of the $\Gamma_{15}-\Delta_1-X_1$ conduction band with the highest valence $\Gamma_{25'}-\Delta_5-X_4$ region (there are eight valence electrons in two formula units of LiAl, which in a diamond-type band structure would occupy the bands up to the $\Gamma_{25'}$ level, leaving a finite $\Gamma_{25'}-\Gamma_{15}$ direct gap and a $\Gamma_{25'}-\Delta_m$ indirect gap). This incipient semiconductor character suggests only small metallic binding in the system.

Figure 8 shows the charge-density differences between the self-consistent variational crystal density $\rho_{\text{crystal}}(\mathbf{r})$ and the superposition density of ground-state neutral Li and Al atoms, along the nearest-neighbor Al-Al, Li-Li, and Li-Al bonds. The small magnitude of these charge-density differences indicate relatively minor rearrangements in the solid (e.g., compare with the difference of 0.096 $e/a.u.$ ³ obtained by Dawson⁵⁹ at the bond center of diamond, using the measured x-ray density in the solid and a superposition of atomic Hartree-Fock carbon densities). The Li-Al bond appears to have an asymmetric build up of charge with greater accumulation towards the Al site, indicating a covalent character with a somewhat larger ionicity towards the Al site. Some charge density is deleted from the bond-edge regions (and from the antibond regions, where the superposition model shows only a low and shallow density) and localized on the atomic sites, with a substantially

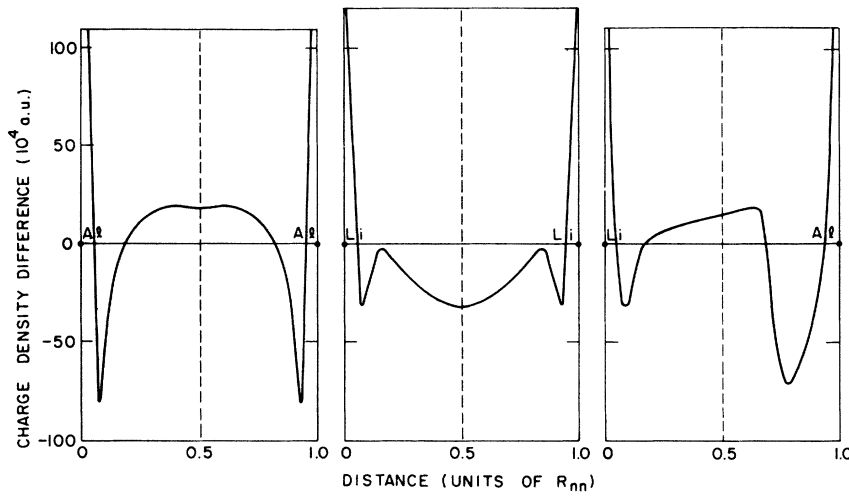


FIG. 8. Charge-density difference between the final self-consistent $\rho_{\text{cry}}(\vec{r})$ and a superposition of neutral ground-state Li and Al densities, along the nearest neighbor Al-Al, Li-Li, and Li-Al bonds. The dashed vertical lines indicate bond centers while the full dots denote the atomic positions. The distance between each pair of atoms is $R_{nn} = \frac{1}{4}\sqrt{3}a$.

larger localization on the Al site than on the Li site. Similar trends have been observed previously in our study of diamond,²¹ where the penetration of charge into the core regions has accounted for a large part of the cohesion of the solid. Thus, the Li-Al bond appears to have a weak covalent character with greater ionic polarization towards the Al site. The Li-Li contacts have significantly lower charge density in the bond region relative to the superposition limit, and are essentially non-bonding. The Al-Al bond appears to have simple metallic character, showing a flat buildup of charge in most of the bond region, together with some charge contraction in the core regions.

In order to gain some insight into the nature of orbital hybridization in the system, we have decomposed the band-by-band charge density into single-site orbital components. Since there is no unique way of partitioning the three-dimensional crystal density into site components, an arbitrary scheme has to be chosen. We prefer the Löwdin population analysis,^{21,60} in which one first transforms the Bloch basis set $\Phi_{\mu\alpha}(\vec{k}, \vec{r})$ into an orthogonal (Wannier-type) basis and then identifies the square of the transformed crystal wave-function expansion coefficients $q_{\mu\alpha}(\vec{k}, j) = |\tilde{C}_{\mu\alpha j}(\vec{k})|^2$ with the contribution of the $|\vec{k}, j\rangle$ state to the μ th orbital charge on site α . Summing on all occupied bands j below the Fermi energy, one obtains the contribution $Q_{\mu\alpha}(\vec{k})$ at point \vec{k} in the BZ of the μ th orbital charge on site α . The sum of $Q_{\mu\alpha}(\vec{k})$ on all orbital indices μ followed by a BZ integral, yields the total electronic charge Q_α on site α due to all band states below the Fermi energy. From this, $\sigma_\alpha = Q_\alpha - Z_\alpha$ then provides a measure of the net ionic charge on site α . Note that contrary to other prescriptions used in muffin-tin studies,⁶¹ no artificial partitioning of space is done here, and similarly,

any shape approximation to $\rho_{\text{cry}}(\vec{r})$ is avoided. Further, in distinction from the Mulliken charge analysis,⁶² the bond charge [e.g., cross terms like $C_{\mu\alpha j}(\vec{k})C_{\mu\beta j}(\vec{k})$] is not partitioned equally between the bonded atoms. One notes, however, that due to the pronounced overlap between the original Bloch basis functions, our transformed Wannier-like functions might possess rather long tails.

Figures 9–11 show the dispersion of the orbital charges $q_{\mu\alpha}(\vec{k}, j)$ for the first four occupied valence bands $j=1$ ($W_1-L_2'-\Gamma_1-X_1$), $j=2$ ($W_1-L_1-\Gamma_{25}'-X_1$), and $j=3, 4$ ($W_2-L_3'-\Gamma_{25}'-X_4$). The lowest valence band (Fig. 9) appears to be of predominantly s character with some buildup of p character towards the hexagonal face at L and the square face at X , similar to the situation in the conduction band of metallic Li (pure Li in a diamond structure would presumably have its Fermi energy at the edge of this band). Strong hybridization of Al and Li states occurs throughout the entire zone. Figure 12 shows the square of the crystal wave func-

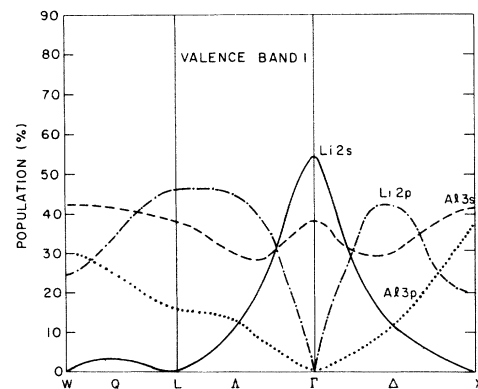


FIG. 9. Orbital charge $q_{\mu\alpha}(\vec{k}, j)$ for the lowest valence band j along the $W_1-L_2'-\Gamma_1-X_1$ line.

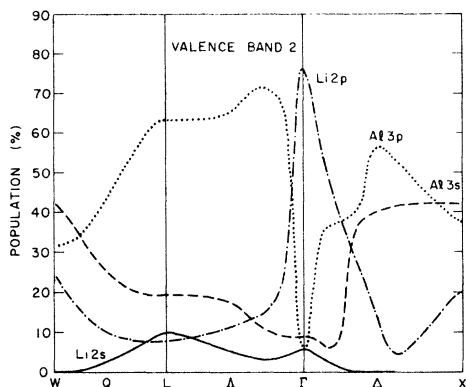


FIG. 10. Orbital charge $q_{\mu\alpha}(\vec{k}, j)$ for the second valence band j along the $W_1-L_1-\Gamma_{25'}-X_1$ line.

tion at the Γ_1 point of this band, where a Li 2s-Li 2s and Al 3s-Al 3s (only the outer nodes of this orbital are shown) character is evident. The Li-Al bond shows similarly s character with some asymmetry towards the Al site. Moving to the second valence band (Fig. 10), a much stronger p character is apparent, with a strong Li contribution near Γ and a predominant Al contribution along the Λ and Δ directions. The Li s character is now strongly reduced in the Δ direction where Al s - p hybrids are predominant. The upper two occupied bands (Fig. 11) are largely of p character in the entire zone, with a strong Li component near the zone center (where the Fermi surface cuts the bands) which decreases rapidly in the Λ and Δ direction, in favor of the Al $3p$ character. The Al $3p$ character in most of the occupied zone for these bands is similar to that obtained in the pure metal (pure Al in a diamond lattice would presumably have its Fermi surface cutting these bands). Figure 13 shows the square of the wave function at $\Gamma_{25'}$, where the Al $3p$ -Li $2p$ mixing is

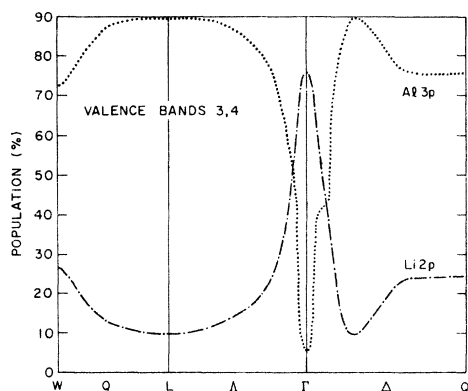


FIG. 11. Orbital charge $q_{\mu\alpha}(\vec{k}, j)$ for the third and fourth valence bands along the $W_2-L_3-\Gamma_{25'}-X_4$ line.

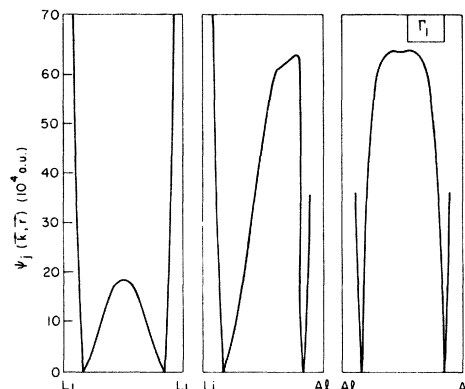


FIG. 12. Square of the crystal wave function at Γ_1 along the Li-Li, Li-Al, and Al-Al bonds.

evident.

Figure 14 shows the dispersion of the *total* orbital charge $Q_{\mu\alpha}(\vec{k})$ due to all bands below ϵ_F as well as that of the net atomic charge σ_α . The system appears to have a Li character around Γ which decreases along the Λ and Δ directions in favor of the Al character that prevails in the entire zone. The Al $3p$ population is significantly larger than in the free ground-state atom ($1e$) while the Al $3s$ population is substantially decreased. The Li population is rather different than in the free ion ($Q_{2s} = Q_{2p} = 0$) or free atom ($Q_{2s} = 1, Q_{2p} = 0$) and shows a significant s to p promotion. There appears to be a significant interatomic charge transfer only around Γ (where the polarity is opposite to that expected from electronegativity considerations due to the higher affinity of Li p state to electron acceptance) while in the rest of the zone the net charges are very small. The BZ integration of these net charges yield the configuration $Li^{+0.07}Al^{-0.07}$ suggesting low ionicity in the system.

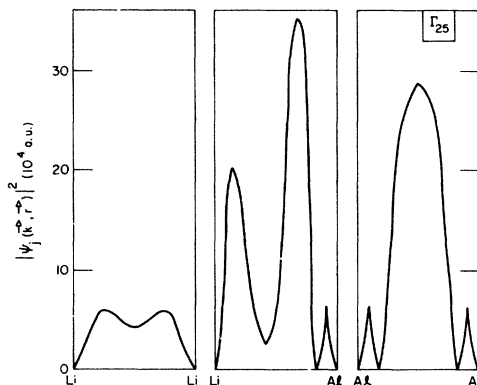


FIG. 13. Square of a representation of the degenerate crystal wave function at $\Gamma_{25'}$ along the Li-Li, Li-Al, and Al-Al bonds.

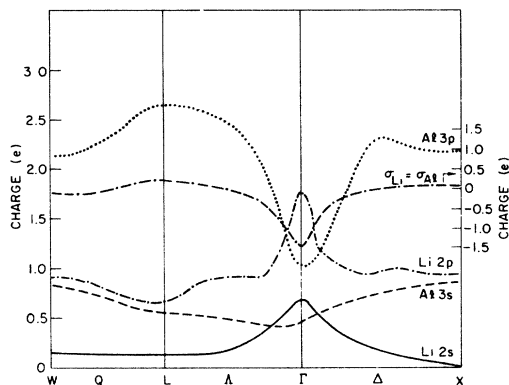


FIG. 14. Dispersion of the total orbital charges and the net atomic charge σ_α due to all occupied bands.

IV. SUMMARY

A fully self-consistent band study on the B32 LiAl structure carried out in the local density formalism indicates that the material is semimetallic due to the overlap of the lowest antibonding p -type band with the upper bonding band along the Γ - X direction. The band structure is qualitatively similar to that characteristic of the covalent IV-IV semiconductors where the systematic decrease in the direct $\Gamma_{25'}-\Gamma_{15}$ and indirect $\Gamma_{25'}-X_1$ gaps along the series shows up in LiAl in a very small direct gap at Γ with a negative indirect Γ - X gap. The lowest part of the occupied bands in LiAl shows strong Al $3s$ -Li $2s$ hybridization, while the s character decreases as one approaches the Fermi energy and finally a predominantly Al $3p$ -Li $2p$ hybrid prevails in the upper portion of the bands. This is consistent with the dramatic reduction in both Li⁷ and Al²⁷ Knight shifts relative to the pure

metals. The density of states at the Fermi level appears to be significantly reduced relative to the pure metals and causes a substantial lowering in the paramagnetic susceptibility. The abrupt decrease in resistivity and decrease in susceptibility as one goes from stoichiometric crystal to a Li-rich crystal is tentatively assigned to the change in position of the Fermi level from the metallic region of the bands in the vacancy-rich stoichiometric crystals to the semimetallic region in the electronically compensated region (Li-rich) characterized by a small Fermi-surface area. The bonding in the material appears to be a composite of a covalent ionic character in the Li-Al bonds and a metallic character to the Al-Al bonds, while the Li-Li contacts are essentially nonbonding. No indication to a Li⁺Al⁻ ionic structure is found; the dominating charge redistribution effects being s to p promotion on both the Li and Al sites with a strong overlap of the Li $2s, 2p$ states with the Al sites simulating an ionic-like charge transfer. Further experiments on the x-ray photoemission spectra, optical transition in the 1-10-eV region as well as low-temperature resistivity and heat-capacity measurement, would be essential to further understand the electronic structure of these materials. The apparent instability that was observed in the differential resistivity measurement around 105 °K clearly calls for more experimental studies on the possible changes in the structure and the phonon spectra.

ACKNOWLEDGMENTS

The author wishes to thank A. H. Switendick for making his preliminary data available and to A. J. Freeman, D. E. Ellis, N. Karnezos, and G. Benesh, for helpful discussions.

*Present address: Department of Physics, University of California, Berkeley, California 94720, U.S.A.

†Support by NSF through the Northwestern University Materials Research Center.

¹E. Zintl and G. Brauer, *Z. Phys. Chem. B* **20**, 245 (1933).

²N. P. Yao, W. J. Walsh, H. Shimotaka, D. J. Arnszen, and P. A. Nelson, Abstract 12, Electrochemical Society Meeting, Boston, 1973 (unpublished).

³H. E. Schone and W. D. Knight, *Acta Metall.* **11**, 179 (1963).

⁴J. R. Willhite, N. Karnezos, P. Cristea, and J. O. Brittain, *J. Phys. Chem. Solids* **37**, 1073 (1976).

⁵J. R. Willhite, N. Karnezos, and J. O. Brittain (unpublished).

⁶R. Messer and F. Noack, *J. Appl. Phys.* **6**, 79 (1975).

⁷L. P. Costas, United States Report, TID-16676 (1962) (unpublished).

⁸A. J. Bradley, H. J. Goldschmidt, and H. Lipson, *J.*

Inst. Met. **63**, 149 (1938).

⁹W. Hume Rothery, J. O. Betterton, and J. Reynolds, *J. Inst. Met.* **80**, 609 (1952).

¹⁰P. Cristea, J. R. Willhite, J. O. Brittain, and C. R. Kannewurf (unpublished).

¹¹W. Klemm and H. Friscke, *Z. Anorg. Allgem. Chem.* **282**, 161 (1955).

¹²U. L. Yao, *Am. Ins. Mining Eng. Res.* **230**, 1725 (1964).

¹³P. Hohenberg and W. Kohn, *Phys. Rev.* **136**, B864 (1964).

¹⁴W. Kohn and L. J. Sham, *Phys. Rev.* **140A**, 1133 (1965).

¹⁵A. Zunger and A. J. Freeman, *Int. J. Quantum Chem. Suppl.* **10**, 383 (1976).

¹⁶A. Zunger and A. J. Freeman, *Phys. Rev. B* **15**, 4716 (1977).

¹⁷P. P. Ewald, *Ann. Phys. (Leipz.)* **64**, 253 (1921).

¹⁸K. S. Singwi, A. Sjölander, P. M. Tosi, and R. H. Land, *Phys. Rev. B* **1**, 1044 (1970); L. Hedin and

B. I. Lundqvist, *J. Phys. C* **4**, 2064 (1971).

- ¹⁹In order to ascertain the effectiveness of the linear basis set and to assure the numerical stability of the calculation, any approximate linear dependence between the Bloch functions has to be eliminated. We find that the Li $2s$, $2p$ Bloch states at the BZ center tend to reproduce each other in a large part of the unit cell volume when the corresponding Bloch sums are carried to convergence. This is primarily induced by the long tails of the atomic Li $2s$ orbitals that tend to shift the $2s$ Bloch function node towards the origin (at points in the zone that are sufficiently far from Γ , interference of these tails due to the Bloch modulation prevents such a linear dependence). To avoid this problem we construct the atomic orbitals by solving self-consistently the atomic LDF equations in the presence of a localizing potential well. The well radius R_w is chosen so that the core orbits would be unchanged in energy and spatial behavior. This is accomplished for $R_w = 10\text{--}13$ a.u. The resulting Bloch orbitals become linearly independent in the entire zone (as can be monitored by the size of the corresponding eigenvalues of the Bloch-overlap matrix).
- ²⁰A. Zunger and A. J. Freeman, *Phys. Rev. B* (to be published).
- ²¹A. Zunger and A. J. Freeman, *Phys. Rev. B* **15**, 5049 (1977).
- ²²A. Zunger and A. J. Freeman (to be published).
- ²³A. Zunger and A. J. Freeman, *Phys. Rev. B* **16**, 906 (1977).
- ²⁴W. P. Menzel, C. C. Lin, D. Fouquet, E. E. Lafon, and R. C. Chaney, *Phys. Rev. Lett.* **30**, 1313 (1973).
- ²⁵C. B. Haselgrove, *Math. Compt.* **15**, 373 (1961).
- ²⁶G. S. Painter and D. E. Ellis, *Phys. Rev. B* **1**, 4727 (1970).
- ²⁷R. C. Chaney, E. E. Lafon and C. C. Lin, *Phys. Rev. B* **4**, 2734 (1971).
- ²⁸J. Callaway and J. L. Fry, *Computational Methods in Band Theory*, edited by P. M. Marcus, J. F. Janak, and A. R. Williams (Plenum, New York, 1971), p. 512.
- ²⁹J. E. Simmons, C. C. Lin, D. F. Fouquet, E. E. Lafon, and R. C. Chaney, *J. Phys. C* **8**, 1549 (1975).
- ³⁰W. Hückel, *Structural Chemistry of Inorganic Compounds* (Elsevier, Amsterdam, 1951), Vol. II, p. 839.
- ³¹D. J. Chadi and M. L. Cohen, *Phys. Rev. B* **8**, 5747 (1973).
- ³²H. J. Monkhorst and J. D. Pack, *Phys. Rev. B* **13**, 5188 (1976).
- ³³G. Lehmann and M. Taut, *Phys. Status Solidi* **54**, 469 (1971).
- ³⁴J. Rath and A. J. Freeman, *Phys. Rev. B* **11**, 2109 (1975).
- ³⁵For review see G. S. Buberger, *Sov. Phys. Usp.* **14**, 180 (1971).
- ³⁶J. R. Chelikowsky and M. Cohen, *Phys. Rev. B* **10**, 5095 (1974).
- ³⁷J. R. Chelikowsky, D. J. Chadi, and M. Cohen, *Phys. Rev. B* **8**, 2786 (1973); F. Herman, R. L. Kortum, and C. D. Kuglin, *Int. J. Quantum Chem. Suppl.* **1**, 533 (1967).
- ³⁸For a review on the optical data, see J. Van Vechten, *Phys. Rev.* **187**, 1007 (1969).
- ³⁹J. R. Chelikowsky and M. Cohen, *Phys. Rev. B* **14**, 556 (1976).
- ⁴⁰C. Carotenuto, E. Colavita, S. Modesti, and M. Sommacal, *Phys. Rev. B* **14**, 5327 (1976).
- ⁴¹L. J. Sham and W. Kohn, *Phys. Rev.* **144**, 390 (1966).
- ⁴²G. S. Painter, D. E. Ellis, and A. R. Lubinsky, *Phys. Rev. B* **4**, 3610 (1971).
- ⁴³H. Basch, A. Viste, and H. B. Gray, *Theor. Chem. Acta* **3**, 358 (1965).
- ⁴⁴W. A. Harrison and S. Ciraci, *Phys. Rev. B* **10**, 1516 (1974); S. Ciraci, *Phys. Status Solidi* **B70**, 689 (1975).
- ⁴⁵C. A. Coulson, L. B. Redeï, and D. Stocker, *Proc. R. Soc. Lond.* **A270**, 357 (1962); L. B. Redeï, *ibid.* **270**, 383 (1962).
- ⁴⁶A. H. Switendick (unpublished results).
- ⁴⁷R. A. Tawil and S. P. Singhal, *Phys. Rev. B* **11**, 699 (1975).
- ⁴⁸J. S. Faulkner, *Phys. Rev.* **178**, 814 (1969); E. C. Snow, *ibid.* **158**, 683 (1967).
- ⁴⁹W. Y. Ching and J. Callaway, *Phys. Rev. B* **9**, 5115 (1974).
- ⁵⁰L. Dagens and F. Perrot, *Phys. Rev. B* **8**, 1281 (1973).
- ⁵¹L. H. Bennett, R. E. Watson, and G. C. Carther, *U. S. Natl. Bur. Stds. report*, 1970 (unpublished).
- ⁵²W. D. Knight, *Solid State Physics*, edited by F. Seitz and D. Turnbull (Academic, New York, 1955), Vol. 2.
- ⁵³J. C. Slater, *Phys. Rev.* **36**, 57 (1930).
- ⁵⁴G. T. Meaden, *Electrical Resistance of Metals* (Plenum, New York, 1965).
- ⁵⁵F. J. DiSalvo, D. E. Moncton, and J. V. Waszczak, *Phys. Rev. B* **14**, 4321 (1977).
- ⁵⁶L. H. Bennett, *Phys. Rev.* **150**, 418 (1966).
- ⁵⁷L. Pauling, *Proc. R. Soc. Lond. A* **196**, 343 (1949).
- ⁵⁸C. Kittile, *Introduction to Solid State Physics* (Wiley, New York, 1968), p. 74.
- ⁵⁹B. Dawson, *Proc. R. Soc. Lond.* **298**, 164 (1967).
- ⁶⁰P. O. Löwdin, *J. Chem. Phys.* **18**, 365 (1950).
- ⁶¹A. Neckel, P. Rastl, R. Wibler, P. Weinberger, and K. Schwarz, *J. Phys. C* **9**, 579 (1976).
- ⁶²R. S. Mulliken, *J. Chem. Phys.* **23**, 1833 (1955).